


Article

Experimental Investigation of Water-Retaining and Mechanical Behaviors of Unbound Granular Materials under Infiltration

Ning Li ^{1,2,*} , Yuxiang Tian ³, Biao Ma ⁴ and Dongxia Hu ⁵¹ School of Civil Engineering, Xi'an University of Architecture and Technology, Xi'an 710055, China² Engineering Research Center of Green Construction & Smart Maintenance of Urban Infrastructure, Universities of Shaanxi Province, Xi'an 710055, China³ Library, Chang'an University, Xi'an 710064, China; yuxiangtian0729@163.com⁴ Highway School, Chang'an University, Xi'an 710064, China; mb@gl.chd.edu.cn⁵ School of Road and Bridge Engineering, Xinjiang Vocational and Technical College of Communication, Urumchi 831401, China; hudongxia_xj@163.com

* Correspondence: lining_sn@xauat.edu.cn; Tel.: +86-137-7252-4365

Abstract: Unbound granular materials (UGM) in permeable pavement will experience large numbers of infiltration during their service-life. The frequently changed moisture not only affects the cooling effect of permeable pavement, but also influences the mechanical behaviors of UGM. However, evidence is lacking to state the influence of infiltration on the behaviors of UGM, which is commonly in fully permeable pavement. Considering the influence of infiltration, this study conducted experimental tests to investigate the effect on the water-retaining and bearing capacity of UGM. With the water-retaining tests, the water-retaining rate in the whole structure and at different depths was analyzed under different infiltration numbers and duration. The results showed that the water-retaining rate increased with the extension of the infiltration duration. The infiltration duration had a significant influence on the water-retaining capacity of UGM, while the infiltration number had little. The difference in the water-retaining rate between the top and bottom layers was up to 2.56%. The water-retaining capacity of the integrated structure was hardly affected due to the dissimilarity of the water-retaining rate at different depths. With infiltrations, the fine aggregate in the upside structure migrated downward to the lower structure, resulting in a reduction in water-retaining rate in the upper structure and an increase at the bottom. In addition, the mechanical behaviors were evaluated by the traditional California Bearing Ratio (CBR) and repeated CBR tests under five infiltrations. The first and second infiltration had a significant influence on the CBR of UGM. With two infiltrations, the plastic strain increased by 57.8% via the repeated CBR tests. The resilient strain had an increase by 36.52% and the equivalent modulus decreased by 28.7% with the first infiltration. The first infiltration presented a critical influence on the bearing capacity of UGM and the effect decreased with the increase in the infiltration number. These findings will enrich the behaviors investigation of UGM and promote its application in the fully permeable pavement.

Keywords: unbound granular materials; permeable pavement; infiltration; water-retaining; CBR; plastic strain; resilient strain



Citation: Li, N.; Tian, Y.; Ma, B.; Hu, D. Experimental Investigation of Water-Retaining and Mechanical Behaviors of Unbound Granular Materials under Infiltration. *Sustainability* **2022**, *14*, 1174. <https://doi.org/10.3390/su14031174>

Academic Editor: Antonio D'Andrea

Received: 20 December 2021

Accepted: 19 January 2022

Published: 20 January 2022

Publisher's Note: MDPI stays neutral with regard to jurisdictional claims in published maps and institutional affiliations.



Copyright: © 2022 by the authors. Licensee MDPI, Basel, Switzerland. This article is an open access article distributed under the terms and conditions of the Creative Commons Attribution (CC BY) license (<https://creativecommons.org/licenses/by/4.0/>).

1. Introduction

Faced with the urban heat island (UHI) effect, permeable pavement has become an important source-control technology for the sponge city under low impact development [1,2]. Large numbers of studies were carried out on the material characteristics [3], functional evaluation [4] and hydraulic properties [5,6] of permeable pavement. Comprehensive analysis methods and a comprehensive evaluation system were put forward on the permeation, retention, storage, purification, usage and drainage of rainfall [6,7].

It is accepted that permeable pavement can lower surface temperature and the UHI effect is alleviated due to the changed water content and heat circulation [2,3]. The cooling

effect can persist if water remains in the internal storage zone of the permeable pavement [7,8]. With porous materials, the pavements could not only improve their own thermal conditions but also can minimize the thermal impacts on the surroundings [9]. The permeable pavements have good permeability so that water can easily enter into and flow out of the structure. Due to frequent contact with water, the hydrological-thermal-mechanical characteristics of permeable pavement are more complicated compared with the traditional non-permeable pavements. Although the properties of the surface layer play a crucial role in permeable pavement [3,10], the water-retaining capacity is limited due to its thin thickness. Additionally, the retained water in the surface is more likely to cause moisture damage under the repeated vehicle loads. However, with the appropriate base/subbase layer, it can provide more space for the retention of water and lower the impact on the surface layer.

To strengthen the sponge effect and the cooling effect of permeable pavement, fully permeable pavements were developed with unbound granular materials (UGM) [11,12]. UGM has the advantage of permeability and drainage, which is one main concern for the current research on UGM used in permeable pavement [12,13]. Hou et al. pointed out that permeable pavement can delay flood peaks due to the existing gravel base course and the drained subgrade [14]. Using an innovation approach, the permeability coefficient of different UGMs was obtained by Li et al. [15]. Kazemi et al. found that the quality of infiltrated water can be improved by base coarse aggregates [16]. On the other hand, several scholars conducted tests about the mechanical properties of UGM used in permeable pavement. Via the full-scale test track with permeable materials, Lu et al. established a prediction model to assess the dynamic response of a UGM layer in a fully permeable road [17]. Ma et al. compared the deformation and resilient modulus of five open-graded base materials, which indicated that UGM used in a base layer can provide good properties for pervious pavement [18]. Sangsefidi et al. investigated the effect of wetting and drying (W-D) cycles on the performance of two aggregates via the California Bearing Ratio (CBR) and repeated load triaxial tests [19]. These findings promote the research and application of fully permeable pavement.

The water content of UGM continually changes in fully permeable pavement. However, current studies did not consider the influence of the changed water on the mechanical properties of UGM. It is unreasonable to analyze the performance of UGM with specific water content. Previous findings have shown that water content and different structure types had significant influence on the bearing capacity of UGM, especially around the optimum moisture content [20,21]. Most results indicated the importance of moisture content on the properties of UGM [22,23]. During rainfall or runoff, the water infiltrates from the upper layer to the lower layer, which will lead to the migration and scouring of particles in the UGM structure. The water would permeate into the UGM layer many times with different durations throughout the whole lifecycle of the fully permeable pavement. The state of moisture content in the UGM layer is dynamic and unknown when the infiltrations occur with different numbers and durations. The condition and effects of the water are always neglected in previous studies on the infiltration.

Considering the effect of the water, most studies concentrated on the permeability and hydraulic conductivity of the materials [24,25]. After rainfall or extensive water sprinkling, some part of the water is drained away by the internal drainage system of permeable pavement, and other part is accumulated in the internal structure which is regarded as the retained water. The retained water in each layer would affect the evaporation rate related to the cooling effect [4,9]. The variation in and distribution of the water in the internal structure influences the thermal conduction of the structure, resulting in temperature variation in the surface [13,26]. Moreover, the composition of the aggregate may be changed during this process, which would influence the water-retaining capacity at different depths. With the changed moisture and aggregate composition, the permanent strain increased and the resilient modulus decreased, which may lead to the damaging of the upper layer [23,27]. Then, the phenomenon of hydro-thermal coupling frequently

appears in permeable pavement [17]. With this consideration, the water-retaining capacity of the UGM can be regarded as an important factor affecting its performance.

The purpose of this study is to investigate the water-retaining and mechanical behavior of UGM under infiltration, as well as aggregate migration. At first, the water-retaining rate was analyzed considering the influence of duration time and numbers of infiltration. Then, the water-retaining rate and aggregate composition at different depths of the specimen were described and analyzed. After that, the traditional CBR and repeated CBR tests were carried out for the UGM with different infiltration numbers. The CBR value, plastic and resilient strains, and equivalent modulus were used to evaluate the influence of infiltration on the bearing capacity of the UGM. The findings in this study provide quantitative evidence to evaluate the influence of infiltration on the water-retaining and mechanical behaviors of UGM, which will benefit the utilization of UGM in fully permeable pavement.

2. Materials and Methods

2.1. Test Materials

The used materials were crushed limestone shipped from a quarry in Tongchuan, Shaanxi. The indicators of the fine and coarse aggregate were tested by the methods in JTGE42-2005 [28], which satisfied the requirements in JTG/T F20-2015 [29]. The test results of the fine and coarse aggregate are listed in Tables 1 and 2.

Table 1. Properties of coarse aggregate.

Indicator	Size of Coarse Aggregate (mm)				
	19–26.5	16–19	13.2–16	9.5–13.2	4.75–9.5
Bulk density (g/cm ³)	2.661	2.657	2.639	2.649	2.62
Vibrated density (g/cm ³)	1.718	1.726	1.732	1.749	1.771
Crushed stone value (%)	\	\	16.5	\	\
Flat and elongated particle content (%)	10.5	9.9	6.9	7.1	4.7
Water absorption (%)	0.62	0.57	0.66	0.61	0.62
Vibrated porosity (%)	35.4	35.0	34.4	34.0	32.4

Table 2. Properties of fine aggregate.

Sand Equivalent (%)	Liquid Limit w_L (%)	Plasticity Index I_P	Mud Content (%)	Water Content (%)	Apparent Density (g/cm ³)	Vibrated Density (g/cm ³)
65.8	17.9	3.2	3.8	2.34	2.661	2.263

The gradation of the used UGM was designed according to the composition of median gradation in JTG/T F20-2015 [29]. With the vibrated compaction method, the maximum dry density and optimum moisture content was 2.311 g/cm³ and 4.8%, respectively. The coefficient of curvature C_c and coefficient of uniformity C_u were 2.53 and 4.18, respectively.

2.2. Test Program

Four types of tests were used to investigate the water-retaining and mechanical behaviors of UGM after the infiltrations, as shown in Figure 1. In the first step, the integrated water-retaining capacity was analyzed considering the infiltration duration time and numbers. According to the previous results in references [30,31], the duration time was divided into three groups, short, median and long with 10, 60, and 240 min, respectively. The infiltration number of the UGM was between 1 and 5. In order to indicate the influence of infiltration, the water-retaining rate and loss of fine aggregate were taken as the indicators. In the second part, the infiltration tests were carried out for 60 min. The specimen was divided into five layers from the top to bottom. In each layer, the water-retaining rate and aggregate composition, along with the depths, were analyzed and compared with the initial state. Then, the traditional CBR tests were conducted at the initial state and after infiltration

for 60 min at different numbers. The influence of the infiltration number on the CBR was analyzed and compared with the previous results. After experiencing 1 to 5 infiltrations, the repeated CBR tests were carried out with 100 loading cycles. The maximum load was 6 kN with a loading rate of 600 N/s. The plastic strain, resilient strain and equivalent modulus were obtained to characterize the bearing capacity of UGM and the influence of infiltration was analyzed. After that, the interaction between the water-retaining and bearing capacity was discussed.

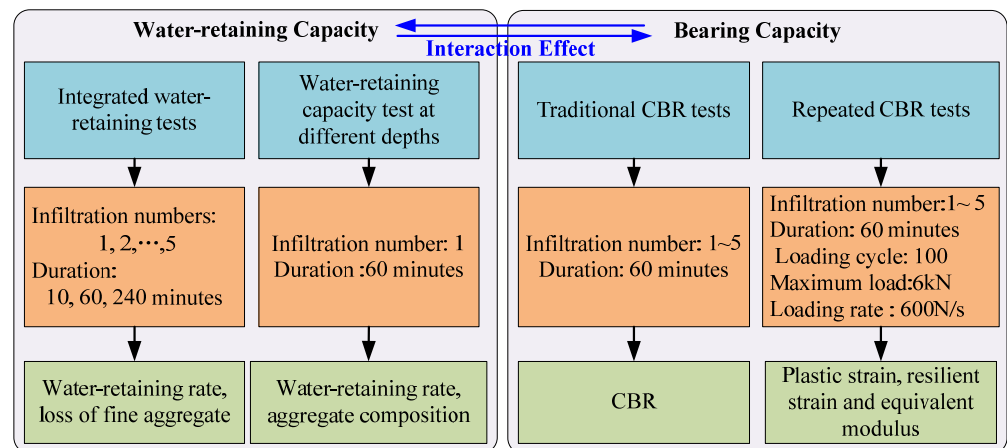


Figure 1. Test program of water-retaining and bearing capacity.

2.3. Test Methods

(1) In order to analyze the water-retaining capacity of UGM after the vertical infiltration, a method similar to that used for porous asphalt mixture [8] was used to simulate the water-retaining capacity after rainfall or runoff. The specific test steps are as follows:

- a. The specimens were prepared in the steel cylinder with 150 mm diameter and 200 mm height. The permeable geotextile was laid at the bottom of the steel cylinder. After being mixed at the optimum moisture content, the granular materials were compacted with vibration in three layers;
- b. The specimen was dried in a 100 °C oven for 12~15 h to avoid the interference of original water. Then, it was weighed at intervals of one hour until the weight was constant. The mass of the specimen was marked as m_D ;
- c. The gap between the specimen and the steel cylinder was filled with water sealing materials. The specimen was supported by a net frame and a recycling bucket was beneath the net frame, as shown in Figure 2. A self-made drip device was used to simulate the infiltration of the water downward from the surface layer. The temperature of the water was kept at 21 ± 1 °C. The infiltration intensity was not considered in this study, and the drip speed was 5 drops per second. The three durations were used for the integrated water-retaining tests. During the infiltration, the flow rate of the water was kept as smooth as possible. It was adjusted frequently so that little water could accumulate on the surface of the specimen. When the infiltration time ended, the total mass of permeable water was recorded as m_A . The infiltration process was finished when no droplets fell from the bottom of the specimen within 15 min. Then, the recycled water in the bucket was weighted as m_R . In addition, the lost fine aggregate was dried and deducted. The water retaining rate S_M of unit mass of the UGM was obtained by Equation (1) as follows

$$S_M = \frac{m_A - m_R}{m_D} \times 100 \quad (1)$$

where S_M is the water retaining rate of UGM, %; m_A is the total mass of infiltrated water, g; m_R is the recycled water during the infiltration process, g; m_D is the mass of the UGM specimen in dry state, g;

- d. After the infiltration, the specimen was carefully moved into a 100 °C oven and dried to a constant weight. Then, the next infiltration was conducted when it cooled to a temperature of 21 ± 1 °C. Following the same operation, the infiltration tests were carried out with five numbers. There were three parallel tests in each infiltration test.

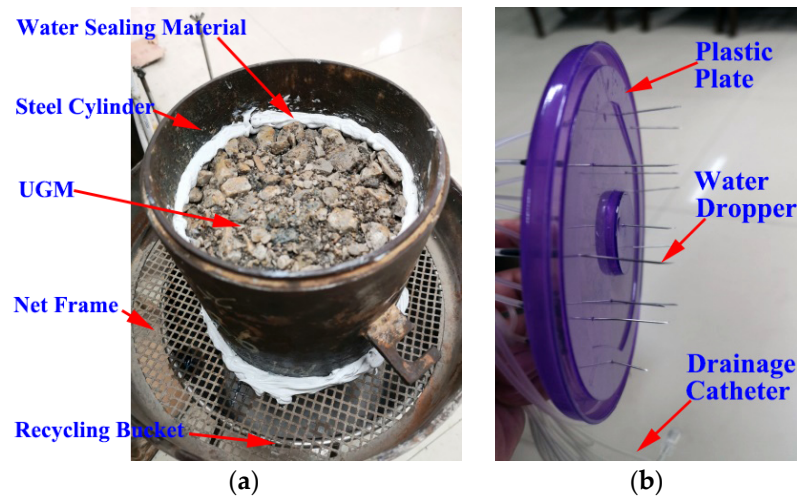


Figure 2. Devices of the water-retaining tests; (a) the specimen on the net frame; (b) self-made drip plate.

(2) Influenced by the migration and scouring from the infiltrated water, the composition of UGM changed at different depths which, in turn, affected the water-retaining capacity. Thus, the water-retaining rate and aggregate composition was calculated at different depths of the specimens.

- a. Two groups of specimens were fabricated in the steel cylinder with 150 mm diameter and 200 mm height. Group A was taken as the control group in the initial state of UGM and group B as the experimental group after the infiltration;
- b. In group B, the infiltration lasted 60 min. at a temperature of 21 ± 1 °C, according to the procedures in (1)c. When the infiltration finished, the specimens had a rest for 60 min. so that the internal moisture tended to be stable. Then, the retained water of two groups at different depths was weighted;
- c. The retained water at different depths was obtained via the stratified sampling method. The locations of sampling started from top to bottom in turns at 0, 50, 100, 150 and 200 mm, respectively. The samples were extracted in the center with a diameter of around 50 mm. Two samples were taken for each layer, and the mass of each sample was about 250 g. The samples were stored in an aluminum box for weighing, and the mass of the water-retained sample was obtained as m_w . Then, the box was moved into the oven at 100 °C with 12 h. The mass of the sample in the dry state was marked as m_d . The water-retaining rate of UGM at different depths was calculated by Equation (2).

$$w = \frac{m_w - m_d}{m_d} \times 100 \quad (2)$$

where w is the water-retaining rate of the sample at different depths, %; m_w is the mass of the sample in water-retaining state, g; m_d is the mass of the sample in dry state, g;

- d. The aggregate composition at different depths was obtained after the infiltration. The aggregate in the dry state was classified into three categories, coarse, median and fine,

which related to particle size in 4.75–19 mm, 1.18–4.75 mm and 0.075–1.18 mm, respectively. At different depths, the mass proportions of the aggregate were calculated before and after the infiltration.

(3) The mechanical behaviors of the infiltrated UGM were investigated using traditional CBR tests and repeated CBR tests. The specimens were prepared at the optimum moisture content via the vibrated method. The test groups experienced 1, 2, 3, 4 and 5 infiltrations, and each infiltration lasted 60 min. The non-infiltration group was conducted as the control test. The traditional CBR and repeated-CBR tests were carried out with three duplications. The CBR tests were performed based on the specifications in JTG E40-2007 [32]. As for the repeated CBR tests, there was no specific protocol in the current test methods. In this study, the repeated CBR tests were conducted with the materials test system (MTS 810) as shown in Figure 3a. The process was referred to from the literature [33,34], which had 100 loading cycles. The maximum axial load was 6 kN, and the minimum load was 45 N. The stress-controlled process was used for the loading and unloading, which had a rate at 600 N/s, as in Figure 3b. In each loading cycle, the plastic and resilient part of the deformation was recorded, as shown in Figure 3c.

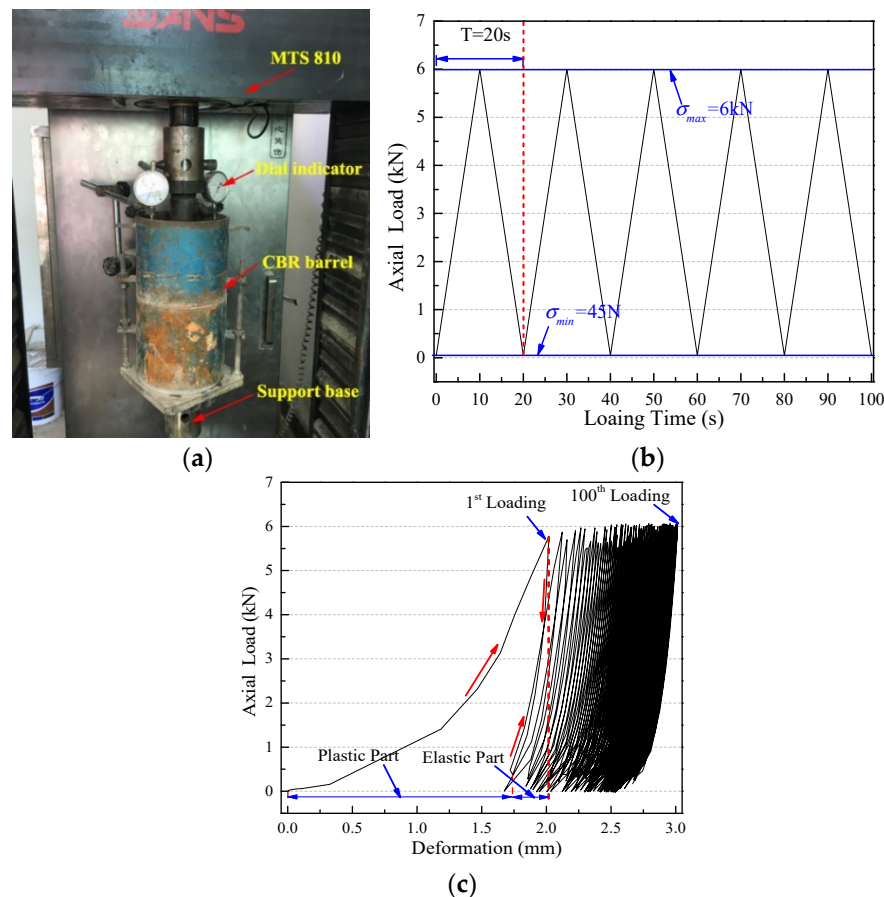


Figure 3. The repeated CBR test; (a) devices of the tests; (b) loading and unloading procedure; (c) recorded data in the tests.

During the repeated CBR tests, plastic and resilient strains were calculated via the curves of the deformation-load. In addition, the equivalent modulus was provided for UGM in the repeated CBR tests [33–35]. Considering the friction between the mould and the UGM, the full-friction and non-friction models were derived as Equations (3) and (4).

$$\text{Full - Friction} \quad E_{equ} = \frac{1.375 \cdot (1 - \mu^{1.286}) \cdot \sigma_p \cdot a}{\omega^{1.086}} \quad (3)$$

$$\text{Non - Friction} \quad E_{equ} = \frac{1.797 \cdot (1 - \mu^{0.889}) \cdot \sigma_p \cdot a}{w^{1.098}} \quad (4)$$

where E_{equ} is the equivalent modulus, MPa; μ is Poisson's ratio of UGM, 0.45; σ_p is the axial stress, MPa; a is radius of the plunger, mm; w is the resilient deformation, mm. Then, the CBR value, plastic and resilient strains and equivalent modulus were used to evaluate the bearing capacity of the UGM.

3. Results

3.1. Water-Retaining Behavior with Five Infiltrations

For the UGM having experienced five infiltrations for 10, 60, and 240 min., the water-retaining rate S_M in the vertical direction and the loss of fine aggregate are shown in Figure 4. With the extension of the duration, the water-retaining rate increased due to the longer infiltration time, as seen in Figure 4a. The duration of infiltration had a significant relationship with the water-retaining capacity of UGM. When the duration time was 10 min, the average water-retaining rate was 3.81% for the five infiltrations. The value for 60 and 240 min. was 4.19% and 4.27%, respectively. Compared with the result at 10 min, the increment of water-retaining rate was 0.33% and 0.46% for 60 and 240 min., respectively. The maximum difference was only 0.08% between 60 and 240 min. The water-retaining rate for 60 min. was greater than that for 10 min.; however, it was similar to the results for 240 min. This showed that the influence on the water-retaining rate decreased as the duration time exceeded 60 min. In addition, the water-retaining rate was smaller than the optimum moisture content (4.8%) of UGM in the three durations. This is due to the fact that some closed pores were formed during the fabrication of the specimens. That the water could not enter into the closed space resulted in a smaller amount of retained water. As for the infiltration number, the water-retaining rate had a slow increase in infiltration number when the duration was 10 min. The mean increment of the water-retaining rate for each infiltration was about 0.075%. As for the infiltration for 60 and 240 min, there was no obvious variation trend for the water-retaining rate during the five infiltrations. The water-retaining rate fluctuated up and down at around 4.2% along with the infiltrations.

With a two-way ANOVA (analysis of variance), the significance of the infiltration numbers and duration was analyzed for the water-retaining rate. When the p -value was smaller than 0.05 for the factor, the hypothesis was accepted, and the factor was regarded as a significant influencing factor on the object. Otherwise, the hypothesis was rejected. At the significance level of 0.05, the p -value was 0.318 and 0.0001 for infiltration numbers and duration. This implies that the infiltration number was not a significant influencing factor on the water-retaining capacity, while the infiltration duration has significant influence on the water-retaining capacity. There are two reasons for this finding: one is that the moisture has a greater opportunity to be attached and absorbed by the aggregate with longer infiltration time, and, also, it can enter into the pores. Another reason is that the aggregate is more likely to migrate given a longer infiltration time. Then, the inner structure is changed and the water-retaining capacity is greater.

With different infiltration durations, the loss of fine aggregate was more obvious in the first two infiltrations, as shown in Figure 4b. In the first two infiltrations, the loss of fine aggregate for 10, 60 and 240 min. accounted for 83%, 85% and 86% of the total loss during the five infiltrations, respectively. Figure 5 shows the recycled water in the first three infiltrations. The clarity of the recycled water is obviously different. With one infiltration, the recycled water was quite turbid with slurry, and it became slightly transparent with a little sediment in the following two infiltrations. After three infiltrations, the loss of fine aggregate was smaller than 1 g. For the Pearson correlation analysis between the water-retaining rate and loss of fine aggregate, the Pearson correlation coefficient at 10, 60 and 240 min was -0.61 , -0.56 and -0.64 , respectively. This showed that the loss and migration of fine aggregate had a strong negative correlation on the water-retaining capacity of the whole structure.

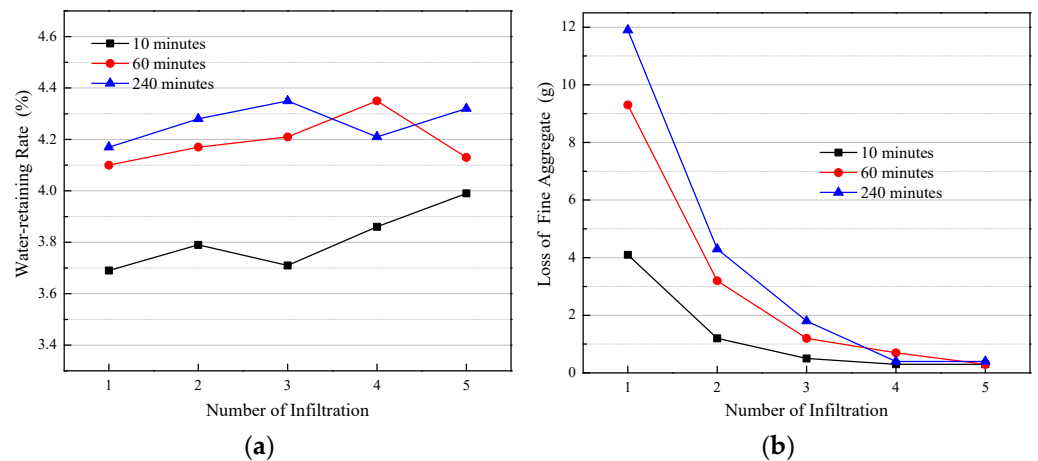


Figure 4. Variation in water-retaining rate and loss of fine aggregate with the infiltration number; (a) water-retaining rate; (b) loss of fine aggregate.

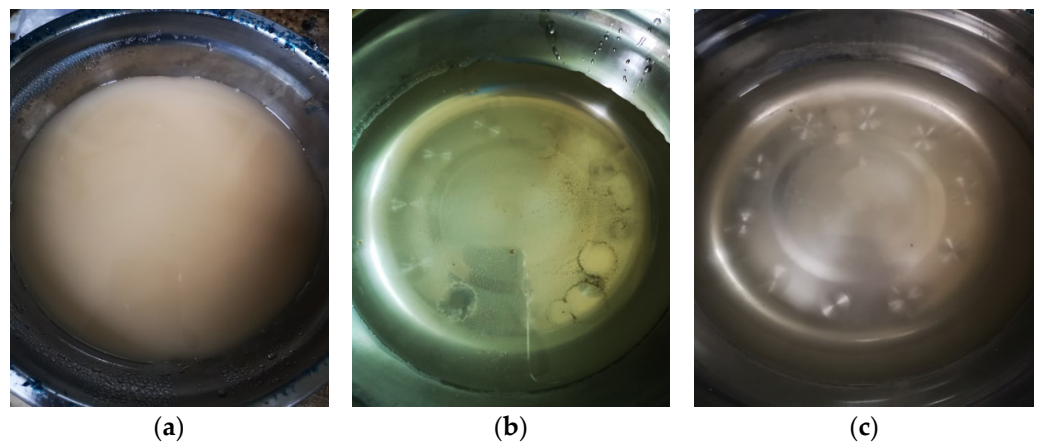


Figure 5. Recycled water in the first three infiltrations for 10 min; (a) the first infiltration; (b) the second infiltration; (c) the third infiltration.

3.2. Water-Retaining Behaviors at Different Depths

Based on the test procedures in Section 2.2, the water-retaining rate in the initial state was marked as w_A , and the water-retaining rate after the infiltration was labeled as w_B . The observations of the stratified sample at different depths were shown in Figures 6 and 7. In the initial state, the coarse, median and fine aggregates displayed the same features at the five depths. After infiltration, the fine aggregate in the upper layer was taken away by the water flow. The top layer displayed more coarse aggregate in the bare state which presented greater pore structure. Some of the fine aggregate was carried away from the top layer, and some of the fine aggregate was taken out of the specimen, causing a small mass of aggregate loss. However, the difference seems unobvious between the initial and infiltration state at different depths, except for the top layer. One reason for this is that the quality of the obtained photos is poor due to the shooting conditions. The shoot section was in the steel cylinder, and the light is restricted with the increase in depth. Then, some shadows appear on the layer surface at different depths.

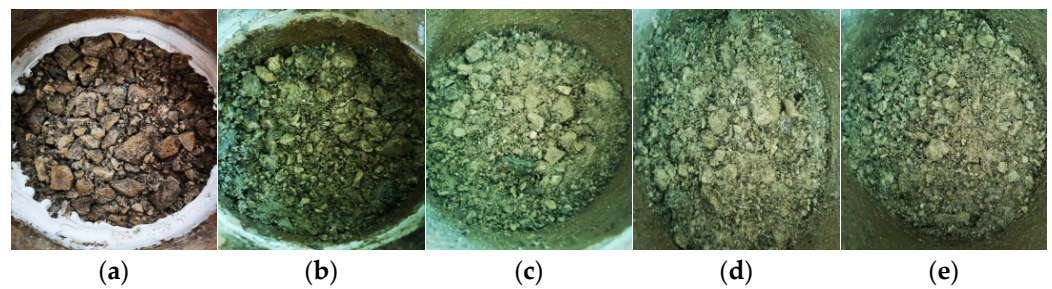


Figure 6. States of stratified samples in the initial state at different depths; (a) 0 mm; (b) 50 mm; (c) 100 mm; (d) 150 mm; (e) 200 mm.

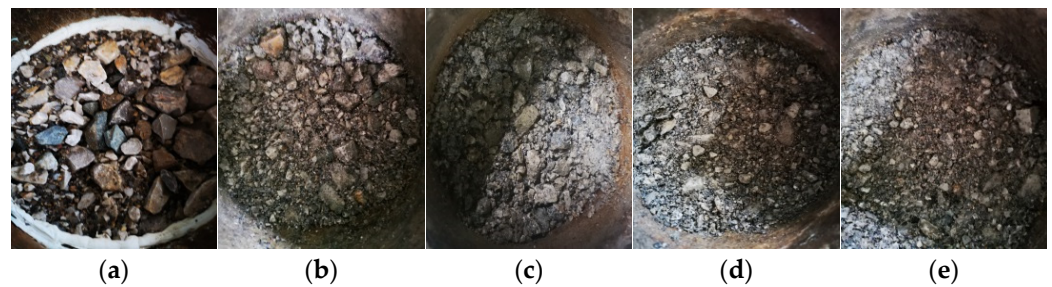


Figure 7. States of stratified samples after infiltration at different depths; (a) 0 mm; (b) 50 mm; (c) 100 mm; (d) 150 mm; (e) 200 mm.

Before and after infiltration, the water-retaining rates w_A and w_B at different depths are shown in Figure 8. In the initial state, the water-retaining rate maintained a stable value at different depths. Although an increasing trend existed from the top to the bottom layer, the variation was relatively small, in which the maximum difference was below 0.7% among the five depths. Based on the variation in the water-retaining rate after infiltration, the sample can be divided into three groups at different depths, upper, middle and lower. In the upper structure, at a depth 0 to 50 mm, the scouring action was obvious due to the flowed water. The number and diameter of pores increased because of the loss and migration of fine aggregate. This provided more channels for the seepage of moisture. However, the pore structure with a greater diameter could not retain enough water in the process of infiltration. Thus, the retained water in the upper group decreased obviously. Compared with the initial state, the reduction of water-retaining rate was 1.17% in the upper layer after infiltration. In the middle layer, the aggregate at the depth of 50 to 100 mm was less affected by water scouring than the upper structure. The composition of the aggregate changed slightly before and after infiltration, resulting in little influence on the structure. Therefore, the change in the water-retaining rate in the middle layer was not obvious. The fine aggregate which migrated from the upper layer affected the structure in the depth of 100 to 200 mm, resulting in the accumulation of fine aggregate in the lower layer. With more fine aggregate, the greater diameter pore was reduced, and the water-retaining capacity was enhanced. Compared with the initial state, the increment of water-retaining rate at 150 mm and 200 mm was 0.35%, and 0.64%, respectively.

The results showed that the changes caused by the infiltration were mainly reflected in the downward migration of fine aggregate during the flow process of water [36,37]. The water-retaining capacity changed at different depths, and the maximum difference in the water-retaining rate between the top and bottom layers was up to 2.56%. However, the average of the water-retaining rate of the whole structure was maintained at 4.01% and 4.03% for the initial and infiltration states. Although the water-retaining rate presented great differences for the two states in different layers, the average of the water-retaining rate of the two states had little difference. This reveals that water-retaining capacity at different layers had a smaller effect on the integrated water-retaining capacity of the structure.

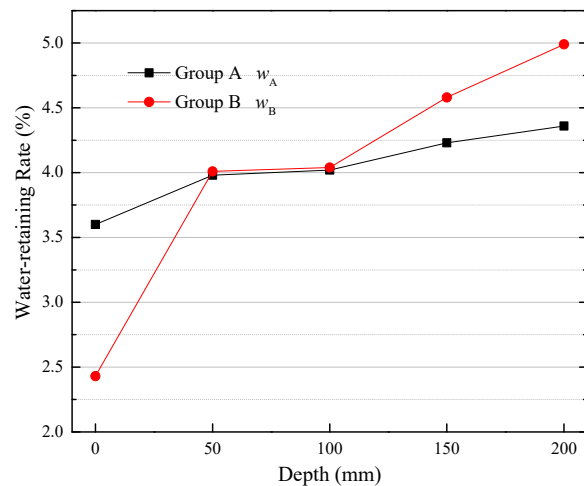


Figure 8. Water-retaining rate of w_A and w_B at different depths.

3.3. Aggregate Composition at Different Depths

Before and after infiltration, the appearance of the three groups of aggregate (coarse, median and fine) was shown in Figure 9. They had the same distribution at different depths before infiltration. However, there was an obvious difference for the distribution after infiltration. At the depth of 0 to 50 mm, the median and fine groups had less aggregate than that at other depths, and the proportion of fine aggregate at 50 to 200 mm was greater than that in the initial state, especially at 150 to 200 mm. After being dried and sieved, the mass proportion of aggregate in the five depths was compared for the three groups.



Figure 9. Sieve results of aggregate at different depths before and after infiltration; (a) the initial state; (b) after infiltration.

Figure 10 shows that the mass proportion of coarse and fine aggregate kept the same state in the five depths for the initial state. The coarse aggregate accounted for

about 61~65% in the five depths, median aggregate accounted for 15~20% and the fine aggregate accounted for 15~18%. The three kinds of aggregate distributed uniformly under the optimum moisture content after mixing and compacting. After infiltration, the fine aggregate migrated from the upper layer and accumulated in the lower layer. Then, the proportion of coarse aggregate increased by 20% in the upper structure and decreased by 15% in the lower structure. The changes in the median aggregate were relatively small at the five depths. The fine aggregate decreased at about 10% in the upper layer and increased by 15% in the lower layer. This reveals that the migration of fine aggregate was significant in the top layer of specimens, which changes the uniformity of gradation distribution.

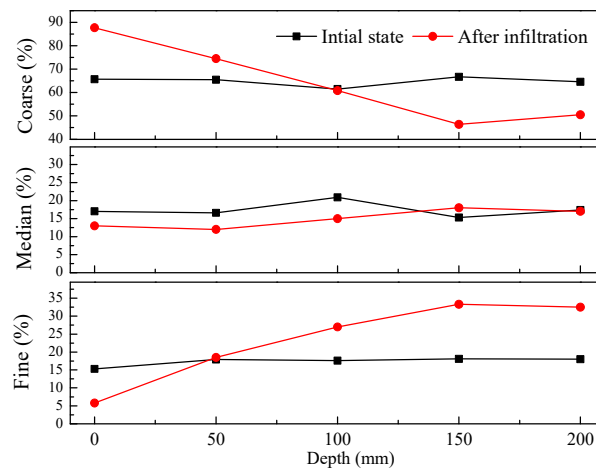


Figure 10. The mass proportion of aggregate at different depths before and after infiltration.

3.4. Mechanical Properties of the Infiltrated UGM

Figure 11 presents the CBR of UGM before and after infiltration. The CBR decreased as the infiltration number increased. The first two infiltrations had an obvious influence on the CBR. Without infiltration, the CBR was up to 113. With one infiltration, the value decreased to 101, and 90 with two infiltrations. The decrease in amplitude accounted for 10.6% and 20.4% deviation from the initial value, respectively. This indicated that the infiltration had a significant effect on the CBR of UGM. After three or more infiltrations, the value maintained at about 90, which tended to be stable. The influence of infiltration on the CBR mainly occurred in the first two infiltrations. This was related to the scouring of the infiltrated water and migration of the fine aggregate. More fine aggregate in the upper layer was taken to the lower layer in the first and second infiltration. Then, there was a greater number of pores in the upper layer, which resulted in a decrease in bearing capacity [36,38]. With three or more infiltrations, the migrated fine aggregate was less, and the aggregate hardly moved in the structure, which was consistent with the observation of the recycled water. Therefore, the bearing capacity of the UGM approached a stable state. In addition, the error bar indicates the variability and repeatability of the results. As seen in Figure 11, the variation amplitude of CBR was up to 20 under different infiltrations, which was due to the great variability of the CBR tests. Although the amplitude was great, the coefficient of variation was smaller than 15%, which can be accepted for civil engineering.

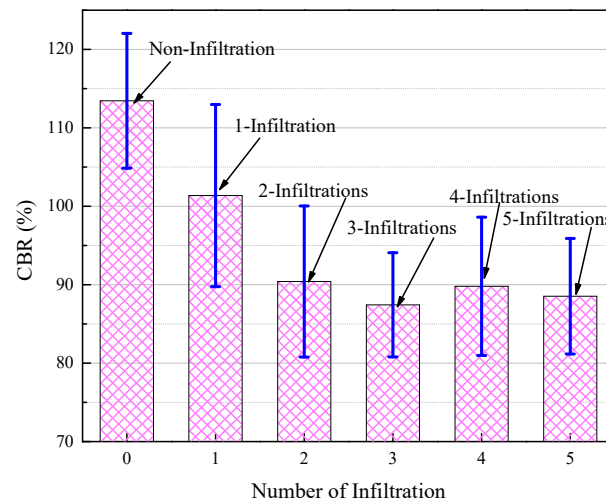


Figure 11. CBR of the UGM with five infiltrations.

With 100 loading cycles, the plastic and resilient strains from the repeated CBR tests are shown in Figure 12. The resilient strain was the mean value from the 60th to 100th loading cycles and the plastic strain was the accumulated strain after 100 loading cycles. For the plastic strain, it presented an increased tendency alongside the increase in infiltration number. Compared with the initial state, the increment of plastic strain was 0.45% with one infiltration, and 0.72% and 0.84% for two and three infiltrations, respectively. The increased amplitude was 36.1%, 57.8% and 67.4%, respectively. This reveals that the infiltration number has a significant influence on the plastic strain of UGM. In addition, the effect of the first infiltration is the greatest, and it decreases alongside the increase in infiltration number. The variation tendency of plastic strain in Figure 12c shows that the plastic strain increased faster with more infiltrations along with the loading cycles. The reasons are also derived from the scouring and aggregate migration caused by the infiltration [38]. Meanwhile, the friction among the aggregate decreased due to the fact that the polishing rate of particles was accelerated with more infiltration under repeated loads in the wet state.

The results in Figure 12b show that the infiltration also had influence on resilient strain. Compared with the initial state, the increment of resilient strain was 0.07% after the first infiltration, which accounted for 36.5% of the initial value. This revealed that infiltration has an obvious influence on the resilient strain. On the other hand, the average of the resilient strain was 0.29% when the UGM experienced different numbers of infiltration. The maximum difference between the mean resilient strains in certain infiltrations was only 0.03%. The variation in resilient strain presented a decreasing trend along with the loading cycle, as shown in Figure 12d. The variation magnitude was up to 0.1% in the first several loading cycles, and it was more obvious in the initial state. With the increase in the loading cycle, the variation in the resilient strain became smaller. The greater variation in the magnitude was related to the loading rate, which was up to 600 N/s. Although the minimum load was set as 45 N, the actual minimum load was not identical and hardly arrived at 45 N during each loading cycle [34]. Likewise, a similar situation occurred under the maximum load condition. Then, the resilient strain may not fully recover, and it changed in each loading cycle. Therefore, the resilient strain had a relative variation along with the loading cycle. This also suggested that the error bar for plastic strain was greater than that of resilient strain. This is related to the test method and the aggregate arrangement of the UGM.

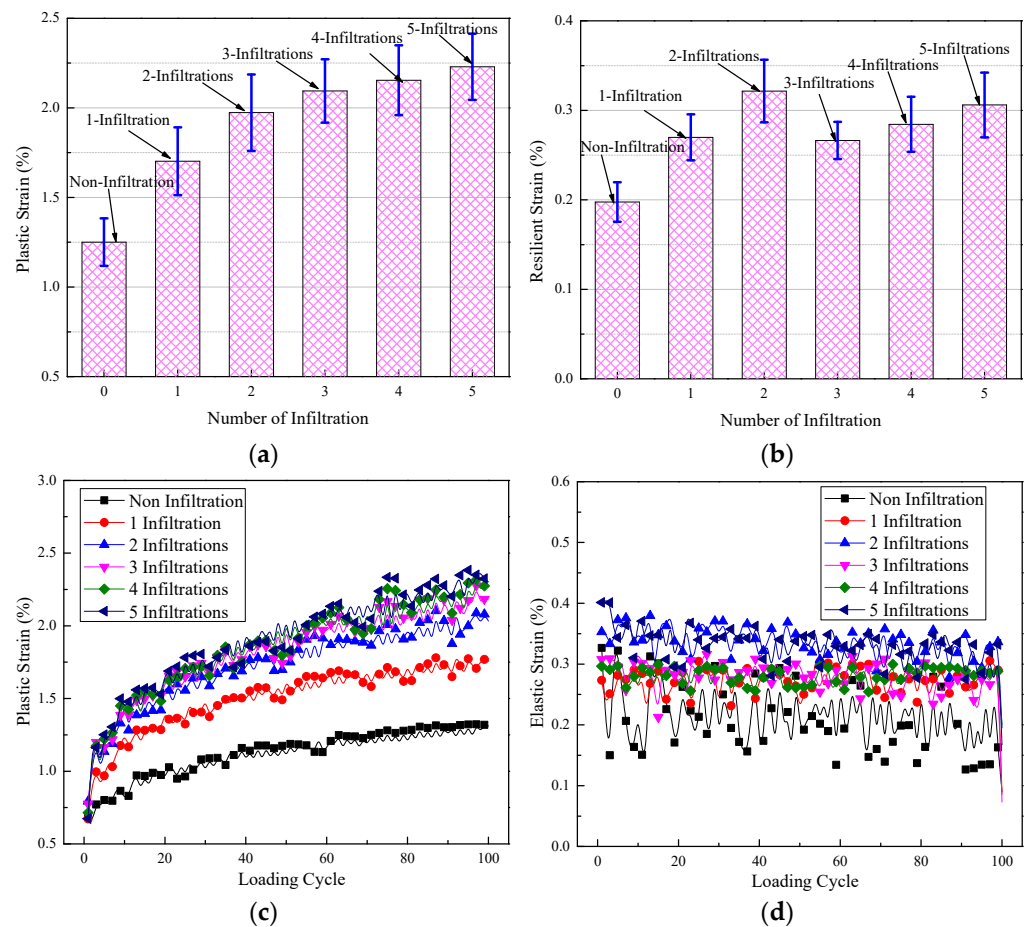


Figure 12. Plastic and resilient strains in the repeated CBR with 100 loading cycles at five infiltrations; (a) plastic strain after 100 loading cycles; (b) resilient strain after 100 loading cycles; (c) plastic strain along with the loading cycle; (d) resilient strain along with the loading cycle.

With the obtained resilient strain, the equivalent modulus can be calculated using Equations (3) and (4), as shown in Figure 13. The equivalent modulus had a contrary trend to the resilient strain, which decreased alongside the increase in infiltration number. With the two models, the modulus obtained from the non-friction model was greater than that from the full-friction one. The two moduli presented a parallel tendency with the variation in infiltration. In previous studies, the resilient modulus of UGM was usually at 200 to 400 MPa [18,39,40]. With Equations (3) and (4), the equivalent modulus was consistent with the existing results for the UGM. However, the modulus was smaller than 200 MPa when the UGM experienced the infiltration. With one infiltration, the modulus decreased by 72.4 MPa (accounted for 28.7% of the initial value) and 76.8 MPa (accounted for 28.9% of the initial value) for the full-friction and non-friction models. The infiltration had an adverse effect on the bearing capacity of UGM. Moreover, the difference between the average and the equivalent modulus with infiltrations was 14.9 MPa and 15.7 MPa for the full-friction and non-friction models, respectively. This suggests that the influence of the infiltration number is not significant, although the first infiltration has a great influence on the equivalent modulus.

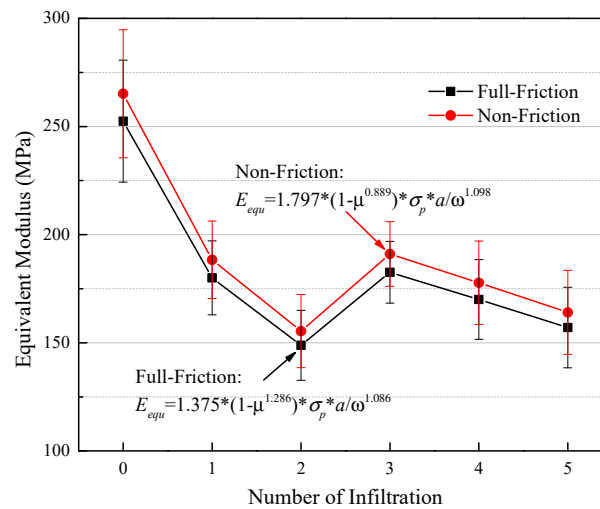


Figure 13. Equivalent modulus with full- friction and non-friction models at the five infiltrations.

3.5. Discussions of Tested Results

The UGM in the fully permeable pavement is usually open-graded without fine aggregate. The runoff can be effectively reduced by the UGM layer during the rainfall because the structure has great porosity as the permeable and reservoir layer [5,18,26]. Then, little water can be reserved in the open-graded UGM layer after the rainfall. Under this condition, the evaporation rate is weakened, leading to the unfavorable cooling effect of the pervious pavement [1,4,13]. Then, the function of water-retaining cannot be neglected for the cooling effect. Currently, the water-retaining capacity of the UGM was hardly emphasized under different infiltration states. The used UGM in this study was the median gradation which belonged to the dense-skeleton grade. It presents some differences with the previous findings about the permeability of the UGM [15,24]. The infiltration numbers had a smaller influence on the water-retaining rate and the effect of duration was significant in a certain range. This is attributed to the migration of the fine aggregate. In the beginning of infiltration, there was some space for the movement of the fine aggregate. In addition, the hydraulic gradients gradually decreased in the vertical direction, resulting in that the movement of fine aggregate was acute in the upper layer and slow in the lower layer [5]. Although the distribution of fine aggregate changed, the loss of fine aggregate was smaller compared to the total mass of the sample. Then, the water-retaining rate was maintained at the same level for the whole structure, although it varied at different depths. The water-retaining rate was highly related to the content of the fine aggregate (as shown in Figure 10), which was explained by Koohmishi [5] and Sangsefidi et al. [19,26].

According to the requirement of the CBR [29], the value should be greater than 120 and 60 for the UGM used in the base and subbase courses, respectively. The obtained CBR in this study ranged from 89 to 113, which could meet the requirement for the subbase course. Regardless of the infiltration, the CBR was high enough for the use of the subbase course. The results showed that the influence of infiltration was limited for the CBR. Namely, the UGM can still be used in the base course if the initial CBR is high enough, which may depend on the gradation design and the maximum size of aggregate [38,39]. However, this may cause a reduction in water-retaining capacity and increase the difficulty of construction. The obtained modulus of UGM was consistent with the value in previous studies which was at 200 to 400 MPa [17,34]. With or without infiltration, the equivalent modulus of the UGM was between 150 to 260 MPa, obtained from the repeated CBR tests. With the infiltration, the modulus was significantly affected, with a decrease at about 30%. Similar to the influence on the CBR, the greatest impact on the equivalent modulus was the first infiltration. The great reduction in the modulus is closely related to the migration of the fine aggregate.

The CBR and plastic strain were compared with the previous study conducted by Sangsefidi et al. [19]. The CBR of the premium aggregates in the dried state was up to 200, which was about 30 greater than that in the optimum moisture content and wet state. With four W-D cycles, the CBR was at about 280 in the dried state, and it was about 220 in the wet state. The results were interesting and surprising. Compared with the results obtained by Sangsefidi et al., the obtained CBR in this study was much smaller and showed a contrary variation tendency. The main reason for the contrary variation tendency was the approach to the wet state of the specimen. In this study, the infiltrated water was dynamic, meaning it would scour and take fine aggregates away. Meanwhile, the water in Sangsefidi et al.'s study was static and the aggregate had little migration. The main reason for the smaller value is that the mass proportion of the fine aggregate CBR in this study was greater than that in Sangsefidi et al.'s study. In addition, the optimum moisture content was also a reason for the noted differences. As for the plastic strain, it was about 0.4–0.5% for the premium aggregates in Sangsefidi et al.'s study with 100 loading cycles and 8 W-D cycles, which was similar to the plastic strain in this study. However, the modulus in the two studies presented a greater difference due to the different test methods. Although Sangsefidi et al. were concerned with the frequent variations of moisture content, the dynamic and flow effect of the infiltrated water was not considered in their studies. The comparisons indicate that some results have a similar value and variation tendency, while others are quite different due to the materials and test methods.

In the fully permeable pavement, the water was drained away in both the vertical and horizontal direction. The drainage in the horizontal direction plays an important role due to the transverse slope [15,26]. In this study, the water entered into and flowed out of the UGM in a free and open state, which can be regarded as the vertical drainage. This was different from the actual pavement. In addition, the permeability of the subgrade was assumed to be great enough so that the water could totally infiltrate at any time. Therefore, the state in this study was an ideal state which only considered the infiltration in the vertical direction and the infiltration intensity was not considered.

4. Conclusions

The water-retaining and mechanical behaviors of UGM were investigated with different infiltration numbers and duration. The water-retaining rate, changes in aggregate composition, CBR, plastic and resilient strain and equivalent modulus were analyzed and discussed. The following conclusions were drawn:

- (1) The water-retaining rate was relatively low for the short-term infiltration, and it gradually increased with the extension of the infiltration duration. The increment of water-retaining rate was up to 0.46% when the duration was extended to 60 min and more. The effect of duration on the water-retaining rate was significant in a certain period, and then it tended to be stable. However, the infiltration numbers had little influence on the water-retaining capacity of UGM;
- (2) The water-retaining rate of stratified samples decreased with the increase in the depth. The difference between the top and bottom of the specimens reached 2.56%. However, the changes in different depths would not affect the integrated water-retaining capacity of the structure. With infiltrations, the fine aggregate migrated downward from the upside to the lower layer. It changed the proportion of fine and coarse aggregate, resulting in a reduction in water-retaining in the upper structure and an increase at the bottom;
- (3) The infiltration number had significant influence on the bearing capacity and plastic strain of UGM, especially in the first and second infiltration. With two infiltrations, the plastic strain increased by 57.8% using the repeated CBR tests. Upon experiencing more infiltrations, the increment of plastic strain tended to be greater along with the loading cycle. After the first infiltration, the resilient strain had an increase of 36.52% and the equivalent modulus decreased by 28.7%. The first infiltration presented a vital

influence on the bearing capacity of UGM, and the effect decreased as the infiltration number increased.

The obtained findings reveal that the infiltration has a significant influence on the water-retaining and bearing capacity of the UGM. However, there are still some limitations in this study. The greatest simplification was that the process in the infiltration tests only considered the penetration in the vertical direction and the infiltration intensity was not included. Secondly, the gradation has an important influence on the water-retaining and mechanical behaviors of UGM. In this study, the median gradation was only used, which did not consider the gradation effect. In addition, the UGM layer lies between the surface and the subgrade layers, which will face non-pressure and pressure conditions. However, only the non-pressure condition was considered in this study. Although some factors are simplified, the findings in this study have revealed the important influence resulting from infiltration. The shortcomings of this study will be the motivations for future studies.

Author Contributions: Conceptualization, N.L. and B.M.; methodology, N.L., Y.T. and B.M.; validation, Y.T. and D.H.; formal analysis, N.L. and Y.T.; investigation, N.L.; resources, N.L. and B.M.; data curation, N.L.; writing—original draft preparation, N.L. and Y.T.; writing—review and editing, B.M. and D.H. All authors have read and agreed to the published version of the manuscript.

Funding: The supports from the Scientific Research Program funded by Shaanxi Provincial Education Department (No. 21JKJ0717), Talent Technology Foundation in Xi'an University of Architecture and Technology (No RC1907) and Project funded by China Postdoctoral Science Foundation (No 2019M663649) are greatly appreciated, as well as Hebei Natural Science Foundation (Grant No. E2019210247.) and Science and Technology Project of Hebei Education Department (Grant No. QN2018238).

Institutional Review Board Statement: Not applicable.

Informed Consent Statement: Not applicable.

Data Availability Statement: The data presented in this study are available on request from the corresponding author.

Conflicts of Interest: The authors declare no conflict of interest.

References

1. Scholz, M.; Grabowiecki, P. Review of permeable pavement systems. *Build. Environ.* **2007**, *42*, 3830–3836. [[CrossRef](#)]
2. Santamouris, M. Using cool pavements as a mitigation strategy to fight urban heat island—A review of the actual developments. *Renew. Sustain. Energy Rev.* **2013**, *26*, 224–240. [[CrossRef](#)]
3. Li, H.; Li, Z.; Zhang, X.; Li, Z.; Liu, D.; Li, T.; Zhang, Z. The effect of different surface materials on runoff quality in permeable pavement systems. *Environ. Sci. Pollut. Res.* **2017**, *24*, 21103–21110. [[CrossRef](#)] [[PubMed](#)]
4. Qin, Y. A review on the development of cool pavements to mitigate urban heat island effect. *Renew. Sustain. Energy Rev.* **2015**, *52*, 445–459. [[CrossRef](#)]
5. Koohmishi, M. Hydraulic conductivity and water level in the reservoir layer of porous pavement considering gradation of aggregate and compaction level. *Constr. Build. Mater.* **2019**, *203*, 27–44. [[CrossRef](#)]
6. Brunetti, G.; Šimůnek, J.; Piro, P. A comprehensive numerical analysis of the hydraulic behavior of a permeable pavement. *J. Hydrol.* **2016**, *540*, 1146–1161. [[CrossRef](#)]
7. Li, H.; Harvey, J.; Ge, Z. Experimental investigation on evaporation rate for enhancing evaporative cooling effect of permeable pavement materials. *Constr. Build. Mater.* **2014**, *65*, 367–375. [[CrossRef](#)]
8. Jiang, W.; Sha, A.; Xiao, J.; Li, Y.; Huang, Y. Experimental study on filtration effect and mechanism of pavement runoff in permeable asphalt pavement. *Constr. Build. Mater.* **2015**, *100*, 102–110. [[CrossRef](#)]
9. Liu, Y.; Li, T.; Yu, L. Urban heat island mitigation and hydrology performance of innovative permeable pavement: A pilot-scale study. *J. Clean. Prod.* **2020**, *244*, 118938. [[CrossRef](#)]
10. Wu, H.; Sun, B.; Li, Z.; Yu, J. Characterizing thermal behaviors of various pavement materials and their thermal impacts on ambient environment. *J. Clean. Prod.* **2018**, *172*, 1358–1367. [[CrossRef](#)]
11. Li, H.; Kayhanian, M.; Harvey, J.T. Comparative field permeability measurement of permeable pavements using ASTM C1701 and NCAT parameter methods. *J. Environ. Manag.* **2013**, *118*, 144–152. [[CrossRef](#)] [[PubMed](#)]
12. Li, H.; Harvey, J.; Jones, D. Cooling effect of permeable asphalt pavement under dry and wet conditions. *Transp. Res. Rec.* **2013**, *2372*, 97–107. [[CrossRef](#)]

13. Qin, Y.; Hiller, J.E. Water availability near the surface dominates the evaporation of pervious concrete. *Constr. Build. Mater.* **2016**, *111*, 77–84. [[CrossRef](#)]
14. Hou, L.; Wang, Y.; Shen, F.; Lei, M.; Wang, X.; Zhao, X.; Gao, S.; Alhaj, A. Study on variation of surface runoff and soil moisture content in the subgrade of permeable pavement structure. *Adv. Civ. Eng.* **2020**, *2020*, 8836643. [[CrossRef](#)]
15. Li, W.; Zheng, N.; Fu, H. Study of drainage performance of graded crushed stone and base drainage system. *J. Highw. Transp. Res. Dev.* **2010**, *27*, 11–16.
16. Kazemi, F.; Hill, K. Effect of permeable pavement basecourse aggregates on stormwater quality for irrigation reuse. *Ecol. Eng.* **2015**, *77*, 189–195. [[CrossRef](#)]
17. Lu, G.; Wang, H.; Törzs, T.; Liu, P.; Zhang, Y.; Wang, D.; Oeser, M.; Grabe, J. In-situ and numerical investigation on the dynamic response of unbounded granular material in permeable pavement. *Transp. Geotech.* **2020**, *25*, 100396. [[CrossRef](#)]
18. Ma, G.; Li, H.; Yang, B.; Zhang, H.; Li, W. Investigation on the deformation behavior of open-graded unbound granular materials for permeable pavement. *Constr. Build. Mater.* **2020**, *260*, 11980. [[CrossRef](#)]
19. Sangsefidi, E.; Larkin, T.J.; Wilson, D.J. The effect of weathering on the engineering properties of laboratory compacted unbound granular materials (UGMs). *Constr. Build. Mater.* **2021**, *276*, 122242. [[CrossRef](#)]
20. Jing, P.; Chazallon, C. Hydro-mechanical behaviour of an unbound granular base course material used in low traffic pavements. *Materials* **2020**, *13*, 852. [[CrossRef](#)]
21. Dan, H.; He, L.; Zhao, L. Experimental investigation on the resilient response of unbound graded aggregate materials by using large-scale dynamic triaxial tests. *Road Mater. Pavement Des.* **2020**, *21*, 434–451.
22. Saevarsdottir, T.; Erlingsson, S. Effect of moisture content on pavement behaviour in a heavy vehicle simulator test. *Road Mater. Pavement.* **2013**, *14*, 274–286. [[CrossRef](#)]
23. Li, N.; Wang, X.; Qiao, R.; Ma, B.; Shao, Z.; Sun, W.; Wang, H. A prediction model of permanent strain of unbound gravel materials based on performance of single-size gravels under repeated loads. *Constr. Build. Mater.* **2020**, *246*, 118492. [[CrossRef](#)]
24. Randolph, B.W.; Cai, J.; Heydinger, A.G.; Gupta, J.D. Laboratory study of hydraulic conductivity for coarse aggregate bases. *Transp. Res. Rec.* **1996**, *1519*, 19–27. [[CrossRef](#)]
25. Kuang, X.; Sansalone, J.; Ying, G.; Ranieri, V. Pore-structure models of hydraulic conductivity for permeable pavement. *J. Hydrol.* **2011**, *399*, 148–157. [[CrossRef](#)]
26. Sangsefidi, E.; Wilson, D.J.; Larkin, T.J.; Black, P.M. The role of water in unbound granular pavement layers: A review. *Transp. Infrast. Geotechnol.* **2019**, *6*, 289–317. [[CrossRef](#)]
27. Li, N.; Ma, B.; Wang, H.; Sun, W. Development of elasto-plastic constitutive model for unbound granular materials under repeated loads. *Transp. Geotech.* **2020**, *23*, 100347. [[CrossRef](#)]
28. State Administration for Market Regulation. *JTG E42-2005, The Methods of Aggregate for Highway Engineering*; China Communications Press: Beijing, China, 2005.
29. State Administration for Market Regulation. *JTG F20-2015, Technical Guidelines for Construction of Highway Roadbases*; China Communications Press: Beijing, China, 2015.
30. Liu, Q.; Liu, S.; Hu, G.; Yang, T.; Du, C.; Oeser, M. Infiltration Capacity and Structural Analysis of Per-meable Pavements for Sustainable Urban: A Full-scale Case Study. *J. Clean. Prod.* **2021**, *288*, 125111. [[CrossRef](#)]
31. Yang, Q.; Beecham, S.; Liu, J.; Pezzaniti, D. The influence of rainfall intensity and duration on sediment pathways and subsequent clogging in permeable pavements. *J. Environ. Manag.* **2019**, *246*, 730–736. [[CrossRef](#)] [[PubMed](#)]
32. State Administration for Market Regulation. *JTG E40-2007, Test Methods of Soil for Highway Engineering*; China Communications Press: Beijing, China, 2007.
33. Araya, A.; Molenaar, A.; Houben, L. Characterization of unbound granular materials using repeated load CBR and triaxial testing. In Proceedings of the GeoShanghai 2010 International Conference, Paving Materials and Pavement Analysis, Shanghai, China, 3–5 June 2010; pp. 355–363.
34. Li, N.; Ma, B.; Wang, H.; Tang, J.; Wang, X.; Shao, Z. Influence of loading frequency on mechanical properties of unbound granular materials via repeated load tests. *Constr. Build. Mater.* **2021**, *301*, 124098. [[CrossRef](#)]
35. Li, N.; Ma, B.; Li, R.; Si, W. Study on Performance of Gravel Aggregate Materials under Single-stage and Multi-stage Loading Modes Based on PUMA. *J. Highway Transp. Res. Dev.* **2019**, *13*, 1–12.
36. Mneina, A.; Shalaby, A. Relating gradation parameters to mechanical and drainage performance of unbound granular materials. *Transp. Geotech.* **2020**, *23*, 100315. [[CrossRef](#)]
37. Törzs, T.; Lu, G.; Monteiro, A.O.; Wang, D.; Grabe, J.; Oeser, M. Hydraulic properties of polyurethane-bound permeable pavement materials considering unsaturated flow. *Constr. Build. Mater.* **2019**, *212*, 422–430. [[CrossRef](#)]
38. Esfahani, M.A.; Goli, A. Effects of aggregate gradation on resilient modulus and CBR in unbound granular materials. *Int. J. Transp. Eng.* **2018**, *5*, 367–381.
39. Su, N.; Xiao, F.; Wang, J.; Amirkhani, S. Characterizations of base and subbase layers for Mechanistic-Empirical Pavement Design. *Constr. Build. Mater.* **2017**, *152*, 731–745. [[CrossRef](#)]
40. Alnedawi, A.; Nepal, K.P.; Al-Ameri, R. Mechanistic behavior of open and dense graded unbound granular materials under traffic loads. *Int. J. Geomate* **2018**, *14*, 124–129. [[CrossRef](#)]